Synthesis, Crystal Structure, EPR and DFT Studies, and Redox Properties of [2]Tetramethyldisilacobaltocenophane

Holger Braunschweig,*[,†] Frank Breher,*[,‡] Martin Kaupp,*[,†] Manuela Gross,[†] Thomas Kupfer,[†] Dominik Nied,[‡] Krzysztof Radacki,[†] and Sandra Schinzel[†]

Institut für Anorganische Chemie, Julius-Maximilians-Universität Würzburg, Am Hubland, D-97074 Würzburg, Germany, and Institut für Anorganische Chemie, Universität Karlsruhe (TH), Engesserstr. 15, D-76131 Karlsruhe, Germany

Received April 29, 2008

The first [2]silacobaltocenophane, $[(Me_2Si)_2(\eta^5\text{-}C_5H_4)_2Co]$ (**1**), was synthesized by dilithiation of 1,2-bis(cyclopentadienyl)-1,1,2,2-tetramethyldisilane with BuLi and subsequent reaction with $[CoBr_2(dme)]$. EPR spectroscopic investigations of frozen pentane solutions of **1** at X-band showed a fully anisotropic **g** tensor ($g_1 = 1.914$, $g_2 = 2.005$, and $g_3 = 2.084$) with hyperfine couplings on all three components ($A_1 = 145$ MHz, $A_2 = 67$ MHz, and $A_3 = 424$ MHz). DFT studies using the B3LYP functional with its 20% exact exchange provide the best agreement with experiment and reproduce the **g** and **A** tensors well. Spin−orbit contributions to the isotropic coupling (A_{PC}) and to the anisotropies ($A_i^{dip,2}$) were found to be significant. As was shown by cyclic voltammetry in THF, **1** is quasi-reversibly oxidized to the neutral cobaltocenium cation $[(Me_2Si)_2(\eta^5\text{-}C_5H_4)_2Co]^+$ (**8**) at a potential of $E^\circ_{1/2} = -1.27$ V (vs the Fc/Fc^+ couple) and quasi-reversibly reduced to the corresponding anion $[(Me_2Si)_2(\eta^5\text{-}C_5H_4)_2Co]^-$ (**9**) at $E^\circ_{1/2} = -2.40$ V. The preparative oxidation of **1** with 1 equiv of ferrocenium hexafluorophosphate ($[Fc][PF_6]$) provided the diamagnetic $[PF_6]^-$ salt of the cation **8** in high yields. The molecular structures of both complexes (**1** and **8**) were confirmed by X-ray diffraction analysis, and a significant decrease in molecular strain was depicted. DFT findings support the experiments.

The structural and electronic properties of strained metallocenophanes as well as their reactivity have attracted a great deal of attention in the last few decades. Strained [1]metallocenophanes have been well investigated, focusing on the cleavage and reactivity of the E−C_{ipso} bond (E = bridging element, C_{ipso} = ipso carbon atom of a cyclopentadienyl ring). In particular, the insertion of late-transition-metal fragments and thermally or nucleophilically induced or metal-catalyzed ring-opening polymerization are of major importance in this context.[1] Furthermore, reactions which decrease the hapticity of the M−C_5H_4 bond from η^5 to a lesser degree of coordination or even involve total elimination of a cyclopentadienyl ring from the metal center in the presence of weak bases are known.[2] Recently [2]metallocenophanes were also studied with regard to the reactivity of the E−E bond toward unsaturated organic substrates in the presence of suitable catalysts. A few examples of oxidative addition of late-transition-metal fragments and subsequent insertions of alkynes or diazo compounds into E−E bonds (E = B, Si, Sn) have been reported up to now.[3] Hence, the synthesis of a variety of [2]metallocenophanes with different bridging moieties and metal centers is of great interest to allow further investigation of their reactivity.

Hitherto only a few examples of paramagnetic group 9 and 10 metallocenophanes have been known. In addition to [2]sila- and [*n*]carbanickelocenophanes (n = 4, 6), strained cobaltocenophanes with C_2 and C_3 bridging units were reported recently.[4] Here we report on the synthesis and characterization of the first disila-bridged cobaltocenophane and its oxidation into the corresponding *ansa*-cobaltocenium hexafluorophosphate.

Results and Discussion

The title compound **1** was synthesized in a straightforward two-step procedure, by lithiation of 1,2-bis(cyclopentadienyl)-1,1,2,2-tetramethyldisilane with BuLi in toluene/ether (9:1) at

* To whom correspondence should be addressed. Fax: +49 931 888 4623 (H.B.). Tel: +49 931 888 5260 (H.B.). E-mail: h.braunschweig@mail.uni-wuerzburg.de, (H.B.); breher@aoc1.uni-karlsruhe.de (F.B.); kaupp@mail.uni-wuerzburg.de (M.K.).

† Julius-Maximilians-Universität Würzburg.

‡ Universität Karlsruhe (TH).

(1) For review articles see: (a) Herbert, D. E.; Mayer, U. F. J.; Manners, I. *Angew. Chem.* **2007**, *119*, 5152; *Angew. Chem., Int. Ed.* **2007**, *46*, 5060. (b) Bellas, V.; Rehahn, M. *Angew. Chem.* **2007**, *119*, 5174; *Angew. Chem., Int. Ed.* **2007**, *46*, 5082. (c) Nguyen, P.; Gomez-Elipe, P.; Manners, I. *Chem. Rev.* **1999**, *99*, 1515. (d) Manners, I. *Chem. Commun.* **1999**, 857. (e) Braunschweig, H.; Breitling, F. M.; Gullo, E.; Kraft, M. *J. Organomet. Chem.* **2003**, *680*, 31. (f) Aldridge, S.; Bresner, C. *Coord. Chem. Rev.* **2003**, *244*, 71. (g) Manners, I. *Polyhedron* **1996**, *15*, 4311.

(2) Herbert, D. E.; Tanabe, M.; Bourke, S. C.; Lough, A. J.; Manners, I. *J. Am. Chem. Soc.* **2008**, *130*, 4166.

(3) (a) Braunschweig, H.; Kupfer, T.; Lutz, M.; Radacki, K.; Seeler, F.; Sigritz, R. *Angew. Chem.* **2006**, *118*, 8217; *Angew. Chem., Int. Ed.* **2006**, *45*, 8048. (b) Braunschweig, H.; Kupfer, T. *J. Am. Chem. Soc.* **2008**, *130*, 4242. (c) Braunschweig, H.; Lutz, M.; Radacki, K *Angew. Chem.* **2005**, *117*, 5792; *Angew. Chem., Int. Ed.* **2005**, *44*, 5647. (d) Braunschweig, H.; Lutz, M.; Radacki, K.; Schaumloeffel, A.; Seeler, F.; Unkelbach, C. *Organometallics* **2006**, *25*, 4433. (e) Herberhold, M.; Steffl, U.; Milius, W.; Wrackmeyer, B. *Angew. Chem.* **1997**, *109*, 1545; *Angew. Chem., Int. Ed.* **1997**, *36*, 1508. (f) Herberhold, M.; Steffl, U.; Wrackmeyer, B. *J. Organomet. Chem.* **1999**, *577*, 76. (g) Finckh, W.; Tang, B. Z.; Lough, A.; Manners, I. *Organometallics* **1992**, *11*, 2904. (h) Braunschweig, H.; Kupfer, T. *Organometallics* **2007**, *26*, 4634.

(4) (a) Braunschweig, H.; Gross, M.; Radacki, K. *Organometallics* **2007**, *26*, 6688. (b) Buchowicz, W.; Jerzykiewicz, L. B.; Krasinska, A.; Losi, S.; Pietrzykowski, A.; Zanello, P. *Organometallics* **2006**, *25*, 5076. (c) Drewitt, M. J.; Barlow, S.; O'Hare, D.; Nelson, J. M.; Nguyen, P.; Manners, I. *Chem. Commun.* **1996**, 2153. (d) Fox, S.; Dunne, J. P.; Tacke, M.; Schmitz, D.; Dronskowski, R. *Eur. J. Inorg. Chem.* **2002**, 3039. (e) Mayer, U. F. J.; Charmant, J. P. H.; Rae, J.; Manners, I. *Organometallics* **2008**, *27*, 1524.

10.1021/om8003724 CCC: $40.75
Publication on Web 11/11/2008

Scheme 1. Synthesis of 1

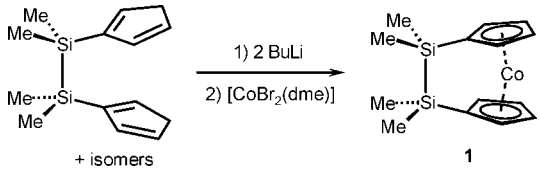

0 °C and successive reaction with $[CoBr_2(dme)]$ at −78 °C in THF (Scheme 1). The product was isolated as an analytically pure, highly air and moisture sensitive dark brown solid in 31% yield. The paramagnetic nature of the 19e species **1** prevented its characterization by NMR spectroscopy in solution. Solution UV−vis spectra of **1** in hexane were recorded in the range from 200 to 600 nm. As expected for cobaltocenes,[5] three characteristic absorptions were observed at 217 nm (ϵ = 18 315 L mol^{-1} cm^{-1}), 268 nm (ϵ = 5210 L mol^{-1} cm^{-1}), and 319 nm (ϵ = 5330 L mol^{-1} cm^{-1}). In comparison, the lowest energy absorbance λ_{max} of $[(H_2C)_2(\eta^5\text{-}C_5H_4)_2Co]$ (**2**) at 486 nm (ϵ = 554 L mol^{-1} cm^{-1}) and the unresolved shoulder around 380 nm of $[(H_2C)_3(\eta^5\text{-}C_5H_4)_2Co]$ (**3**) show a red shift relative to that of **1** (319 nm).[4e] This significant red shift correlates with the increasing molecular ring strain which has already been reported for trochrocenophanes. This effect can be explained by a lowering of the HOMO−LUMO energy difference with increasing tilt angles. Only a few bridging substituents such as B═NR_2 deviate from this trend due to the influence of the bridging moiety on the electronic structure of the metal complexes.[6]

Solutions of **1** in pentane are EPR silent at room temperature. As is known for many other Co(II) compounds, the short spin−lattice relaxation time makes signal recording difficult in the room-temperature region.[7] However, samples of **1** show strong signals in frozen solution already upon cooling to 100 K. Figure 1 summarizes the CW EPR spectra of **1** in pentane recorded at X-band, along with the corresponding simulations for a system with an electron spin of $S = {}^1/_2$. Only some minor features of the experimental spectrum could not be reproduced by the simulation. Further improvement by iterative optimization of the parameters failed and only yielded an unrealistically large line width for L_1. The spin Hamiltonian parameters used for the simulations are $g_1 = 1.914$, $g_2 = 2.005$, and $g_3 = 2.084$, with a hyperfine coupling to the Co(II) ion ($I = {}^7/_2$) of A_1 = 145 MHz, A_2 = 67 MHz, and A_3 = 424 MHz. This is in accord with DFT calculations, which predict the spin density to reside mainly on the Co atom and in p-type orbitals of the C_5H_4 carbon atoms attached to the silicon bridge.

The g values and ^{59}Co hyperfine couplings A are compared in Table 1 with those of other selected Co(II) Cp complexes. In D_{5d} symmetry, cobaltocene itself has a $^2E_{1g}$ ground state (electronic configuration $(e_{2g})^4(a_{1g})^2(e_{1g})^1$) owing to the orbital degeneracy of the e_{1g} orbital set. EPR signals are observed only at very low temperatures (4 K), due to the short relaxation times associated with the degenerate ground state. Under pure axial symmetry, $g_\perp$ for the $^2E_{1g}$ metallocenes would be zero and no EPR signal is expected.[7,8] Experimentally, the EPR parameters of cobaltocene and related Jahn−Teller-active systems (Table 1) are markedly anisotropic and are dramatically affected by the matrix (crystalline host lattices and rare-gas matrices; single crystals or powders).[8] A fully anisotropic **g** tensor (rhombic spectrum, i.e. $g_1 \neq g_2 \neq g_3$), with all three g values significantly below the free-electron value and generally with hyperfine couplings on all three components, is usually observed. Detailed studies of the electronic structure of cobaltocenes performed in seminal work by Ammeter et al. indicate that dynamic Jahn−Teller distortions predominate over static distortions but are gradually suppressed (relative to the static distortion) by the increasing asymmetry of the guest molecule and/or host lattice.[8,9] Lowering the ligand field symmetry increases the splitting of the e_{1g} pair, the relaxation times, and the g values.

As one might expect from a qualitative MO diagram for a bridged *ansa*-cobaltocene such as **1**, the orbital degeneracy of the e_{1g} state is lifted (symmetry C_{2v} or lower). In fact, the observed **g** tensor of **1** differs strongly from those of the nonbridged cobaltocenes (Cp_2Co (**4**), Cp^*_2Co (**5**); cf. Table 1),[8,10] by exhibiting lower anisotropy with one value below, one above, and one near g_e. The data are more in line with those for half-sandwich complexes of Co^{II} (**6**, **7**) than with those for genuine cobaltocenes.[11] As mentioned above, the hyperfine data of Cp_2Co (**4**) or Cp^*_2Co (**5**) vary in a large range depending on environment. Here the data of **1** fit in better but are also consistent with the half-sandwich complexes **6** and **7** (albeit with a somewhat larger maximum component).

Our DFT calculations reproduce the **g** tensor of **1** well. Table 2 shows the performance of different exchange-correlation functionals differing in exact-exchange admixture between 0% (BLYP) and 50% (BHLYP). While for early (V) or late (Cu) 3d transition-metal complexes our experience indicated the best performance with exact-exchange admixtures above 30%,[12] it is known that, for complexes of Fe or Co, these large admixtures may deteriorate results due to the onset of spin contamination.[13] This case seems to be just reached for **1**, as indicated by the $\langle S^2 \rangle$ expectation values provided, which start deviating more from the nominal 0.75 as the exact-exchange admixture is increased. Overall, the B3LYP functional with its 20% exact exchange provides the best agreement with experiment.

The absolute value of the largest **A**-tensor component (A_1) is also reproduced well, and all three hyperfine tensor components are predicted to be negative. However, the values of the two smaller components are not reproduced as well by any of the functionals. We note furthermore that spin−orbit contributions to the isotropic coupling (A_{PC}) and to the anisotropies ($A_i^{dip,2}$) are significant. Interestingly, the overall A_{iso} becomes only somewhat more negative from BLYP to B3LYP and then stays

(5) Ketkov, S. Y.; Domrachev, G. A. *Inorg. Chim. Acta* **1990**, *178*, 233.
(6) (a) Berenbaum, A.; Braunschweig, H.; Dirk, R.; Englert, U.; Green, J. C.; Jakle, F.; Lough, A. J.; Manners, I. *J. Am. Chem. Soc.* **2000**, *122*, 5765. (b) Braunschweig, H.; Kupfer, T.; Lutz, M.; Radacki, K. *J. Am. Chem. Soc.* **2007**, *129*, 8893.
(7) Abragram, A.; Bleaney, B. *Electron Paramagnetic Resonance of Transition Ions*; Oxford University Press (Clarendon): Oxford, U.K., 1970.
(8) (a) Ammeter, J. H.; Swalen, J. D. *J. Chem. Phys.* **1972**, *57*, 678. (b) Ammeter, J. H.; Brom, J. M. *Chem. Phys. Lett.* **1974**, *27*, 380. (c) Ammeter, J. H.; Oswald, N.; Bucher, R. *Helv. Chim. Acta* **1975**, *58*, 671. (d) Ammeter, J. H. *J. Magn. Reson.* **1978**, *30*, 299.
(9) Weber, J.; Goursot, A.; Pénigault, E.; Ammeter, J. H.; Bachmann, J. *J. Am. Chem. Soc.* **1982**, *104*, 1491.
(10) (a) Zoller, L.; Moser, E.; Ammeter, J. H. *J. Phys. Chem.* **1986**, *90*, 6632. (b) Robbins, J. L.; Edelstein, N.; Spencer, B.; Smart, J. C. *J. Am. Chem. Soc.* **1982**, *104*, 1882.
(11) (a) Brunker, T. J.; Green, J. C.; O'Hare, D. *Inorg. Chem.* **2003**, *42*, 4366. (b) Smith, M. E.; Anderson, R. A. *J. Am. Chem. Soc.* **1996**, *118*, 11119.
(12) (a) Remenyi, C.; Munzarova, M. L.; Kaupp, M. *J. Phys. Chem. B* **2005**, *109*, 4227. (b) Remenyi, C.; Reviakine, R.; Kaupp, M. *J. Phys. Chem. A* **2006**, *110*, 4021. (c) Remenyi, C.; Reviakine, R.; Kaupp, M. *J. Phys. Chem. B* **2007**, *111*, 8290. (d) Braunschweig, H.; Kaupp, M.; Adams, C. J.; Kupfer, T.; Radacki, K.; Schinzel, S. *J. Am. Chem. Soc.* **2008**, *130*, 11376.
(13) Munzarová, M.; Kaupp, M. *J. Phys. Chem. A* **1999**, *103*, 9966.

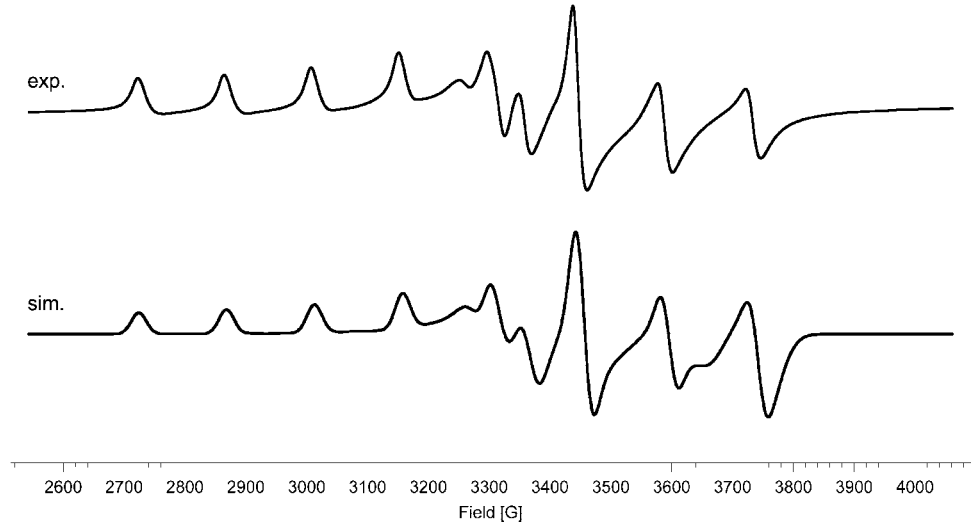

Figure 1. Experimental (exp.) and simulated (sim.) CW EPR spectra of **1** in pentane (frozen solution) at 100 K at X-band.

Table 1. EPR Spectroscopic Data for 1 and Selected Co(II) Cp Compounds (Cp = C_5H_5, Cp* = C_5Me_5, Tp = Tris(pyrazolyl)hydroborate, acac = Acetylacetonate)[a]

compd	g_1	g_2	g_3	A_1	A_2	A_3	ref
1	1.914	2.005	2.084	145	67	424	this work
Cp_2Co[a] (**4**)	1.755	1.847	1.693	n.a.	484	252	8
Cp_2Co[b] (**4**)	1.140	1.219	1.585	71	338	83	8
Cp^*_2Co[c] (**5**)	1.676	1.737	1.721	34	380	235	10
Cp^*_2Co[d] (**5**)	1.935	1.992	1.772	79	402	208	10
[CoCp*Tp] (**6**)	1.971	2.086	2.177	90	62	235	11a
[CoCp(acac)] (**7**)	1.970	2.091	2.241	111	n.a.	309	11b

[a] Hyperfine couplings to ^{59}Co are given in MHz. The axes are not assigned, except for the data of Cp_2Co (**4**) and Cp^*_2Co (**5**). Legend for different host lattices: (a) Cp_2Fe; (b) Cp_2Ru; (c) Cp^*_2Fe; (d) Cp^*_2Ru. See cited references for more details and other conditions.

almost constant with larger exact exchange (Table 2). This is due to a compensation between a more negative A_{FC} (due to an enhancement of the overall negative core−shell spin polarization contributions to the spin density at the nucleus[13,14]) and a more positive A_{PC} (the spin−orbit contributions increase as the spin density on Co increases; Table 2). The *A*-anisotropy values A_i feature a similar but less pronounced compensation between the exact-exchange dependences of nonrelativistic first-order contributions T_i and second-order spin−orbit contributions $A_1^{dip,2}$ (Table 2).

Interestingly, the computations on the parent Cp_2Co (**4**) provide **g** and **A** tensors very similar to those for **1**. While the latter agree well with experiment, this is not the case for Cp_2Co (**4**) (Table 2). It must be presumed that the unusually large *g* anisotropies and their large dependences on the host matrix for Cp_2Co (**4**) and Cp^*_2Co (**5**) (Table 1) are due to the previously discussed[8] dynamic Jahn−Teller distortion in those systems.[10b] Our computations confirm the dynamic Jahn−Teller distortion: the full structure optimizations provide a slightly distorted C_s-symmetrical minimum structure. However, its energy is only about 0.1 kJ mol^{-1} lower than that of the minimum structure at D_{5d} symmetry. This difference is less than the zero-point vibrational energy difference of 0.6 kJ mol^{-1}, consistent with the absence of a static distortion. Discussion of the precise reasons for the magnitudes and directions of the dramatic matrix effects on the **g** tensor is beyond the scope of this work. It should suffice to note that the bridged cobaltocene **1** behaves "normally", and its **g** tensor is well reproduced by DFT calculations. In contrast, the **g** tensor of Cp_2Co (**4**) is obviously abnormal in the sense of effects arising from the dynamical Jahn−Teller distortion.

Cobaltocenes are readily available metal sandwich complexes of moderate redox strength ($E°_{1/2}(Co^{II}/Co^{III}) \approx -1.3$ V), and due to this they have become very powerful one-electron reducing reagents.[15] In order to obtain the electrochemical characteristics of **1**, we investigated THF solutions of the latter by using cyclic voltammetry (solid line in Figure 2). At room temperature, **1** is quasi-reversibly oxidized to the neutral cobaltocenium cation **8** at a potential of $E°_{1/2} = -1.27$ V (vs the Fc/Fc^+ couple). For the complementary reduction, a second quasi-reversible redox wave is observed for the process $[(Me_2Si)_2(\eta^5\text{-}C_5H_4)_2Co]$ (**1**) + $e^- \rightleftarrows [(Me_2Si)_2(\eta^5\text{-}C_5H_4)_2Co]^-$ (**9**) at $E°_{1/2} = -2.40$ V. Both half-wave potentials are comparable to those found for the Cp_2Co (**4**) parent compound (cf. $E°_{1/2} = -1.3$ V and $E°_{1/2} = -2.2$ V).[16,20] The disproportionation constant K_{disp} for the reaction 2 $[(Me_2Si)_2(\eta^5\text{-}C_5H_4)_2Co]$ (**1**) $\rightleftarrows$ $[(Me_2Si)_2(\eta^5\text{-}C_5H_4)_2Co]^+$ (**8**) + $[(Me_2Si)_2(\eta^5\text{-}C_5H_4)_2Co]^-$ (**9**) was calculated to be 3.7×10^{-20}. This observation indicates the high thermodynamic stability of the *ansa*-cobaltocene **1**. The differences of the peak potentials $\Delta(\varphi_p{}^a - \varphi_p{}^c)$ for each redox wave in THF are comparable ($\Delta\varphi_p(1) = 160$ mV, $\Delta\varphi_p(2) = 166$ mV).[17] For electrochemical studies of the corresponding cationic counterpart (i.e., **8**) in acetonitrile, see below.

Since both redox waves behave quasi-reversibly, some moderate structural changes may be anticipated.[18] This suggestion was supported by DFT findings, the main results of which are compiled in Figure 3 (see also the Supporting Information). The calculated bond lengths and angles of **1** and **8** nicely reproduce the structural parameters observed by X-ray diffraction (vide infra). Since the SOMO of **1** is $Co-C_{Cp}$ antibonding in nature (e.g., $d(Co-X_{cent}) = 172.1$ pm), all metal−carbon distances are considerably shorter in the oxidized form (**8**, $d(Co-X_{cent}) = 164.3$ pm). The same tendency is observed for the Si−Si bond length. Pertinent structural

(14) Malkin, V. G.; Malkina, O. L.; Casida, M. E.; Salahub, D. R. *J. Am. Chem. Soc.* **1994**, *116*, 5898.

(15) Connelly, N. G.; Geiger, W. E. *Chem. Rev.* **1996**, *96*, 877.

(16) (a) Geiger, W. E. *J. Am. Chem. Soc.* **1974**, *96*, 2632. (b) El Murr, N.; Dabard, R.; Laviron, E. *J. Organomet. Chem.* **1973**, *47*, C13.

(17) We are not discussing rate constants and and thermodynamic parameters in detail because uncompensated solution resistance R_u and other factors of our experimental setup have a strong influence.

(18) Geiger, W. E. *Organometallics* **2007**, *26*, 5738.

Table 2. Computed and Spectroscopic EPR Data for 1 and 4[a]

compd		g_{iso}	g_1, g_2, g_3	A_{iso}	A_1, A_2, A_3	A_{FC}	$T_1, T_2, T3$	A_{PC}	$A_1^{dip,2}, A_2^{dip,2}, A_3^{dip,2}$	$\langle S^2 \rangle$	ρ(Co)
1	BLYP	1.991	1.899, 2.013, 2.059	−129	−357, −45, 15	−140	−281, 145, 136	10	63, −51, 18	0.760	0.713
	B3LYP	2.008	1.891, 2.036, 2.099	−160	−395, −80, −4	−186	−308, 166, 143	26	99, −59, 39	0.772	0.830
	B30LYP	2.022	1.892, 2.052, 2.122	−167	−403, −91, −7	−204	−319, 174, 145	38	121, −61, 53	0.778	0.878
	B40LYP	2.039	1.893, 2.071, 2.151	−170	−402, −102, −4	−221	−329, 181, 147	51	147, −63, 70	0.785	0.919
	BHLYP	2.056	1.895, 2.090, 2.181	−170	−399, −113, 2	−235	−337, 186, 151	65	173, −64, 86	0.790	0.946
	exptl	2.001	1.914, 2.005, 2.084	|212|	|424|, |145|, |67|						
4	BLYP	1.974	1.860, 2.012, 2.050	−142	−372, −66, 13	−145	−289, 149, 140	3	62, −70, 18	0.758	0.718
	B3LYP	1.993	1.856, 2.035, 2.089	−171	−408, −99, −7	−191	−314, 169, 145	19	96, −77, 39	0.769	0.829
	B30LYP	2.009	1.864, 2.051, 2.112	−177	−415, −107, −8	−209	−324, 177, 147	32	118, −76, 53	0.774	0.874
	B40LYP	2.028	1.870, 2.071, 2.141	−178	−413, −116, −5	−225	−333, 184, 149	46	144, −76, 71	0.780	0.917
	BHLYP	2.046	1.876, 2.091, 2.171	−178	−409, −125, 2	−238	−342, 188, 153	61	171, −76, 87	0.783	0.940
	exptl	1.765	1.693, 1.755, 1.847		484, 252, n.a.						
	exptl	1.315	1.140, 1.219, 1.585	|164|	|338|, |83|, |71|						

[a] Hyperfine couplings to ^{59}Co are given in MHz. g_{iso} is the absolute isotropic g value and g_i the anisotropic part. A_{iso} is the total isotropic value, A_i represents the anisotropic part of the full **A** tensor, and A_{FC} and A_{PC} denote the isotropic first-order Fermi-contact and second-order pseudocontact (spin−orbit) contributions to the full total **A** tensor, respectively. T_i and $A_i^{dip,2}$ denote respectively the first-order nonrelativistic and second-order spin−orbit anisotropic tensors. ρ(Co) is the Mulliken spin density of Co.

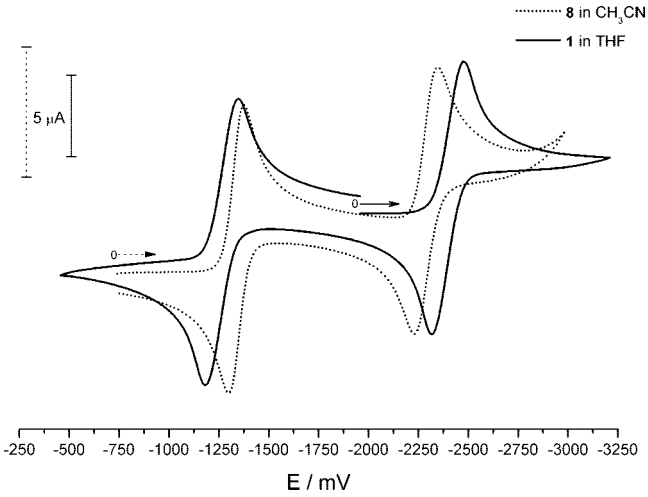

Figure 2. Cyclic voltammetry of **1** (solid line) and **8** (dotted line) at room temperature in THF (**1**) and acetonitrile (**8**) vs Fc/Fc$^+$ (scan rate 100 mV s^{-1}, Pt/[nBu$_4$N][PF$_6$]/Ag). The intensities of the current peak potentials were scaled for comparison. Both redox waves show completely the same behavior in a second CV cycle; only one is shown here. One irreversible redox process at a positive potential of $E^0_{1/2} \approx +1.74$ V for **8** in acetonitrile is not shown for clarity (see text for details).

parameters to describe the strain in *ansa*-metallocenes are the tilt angle α (defined as the angle between the two cyclopentadienyl ring planes) and the distortion δ ($X_{cent}1-M-X_{cent}2$). As expected, a smaller tilt angle α and a larger value for δ are calculated for **8**. Upon one-electron reduction of **1** to the anionic compound **9**, the Co−C_{Cp} distances change considerably (d(Co-X_{cent}) = 184.5 pm), the tilt angle α becomes larger (9.6°), and the C_5H_4 rings deviate from the ideal eclipsed arrangement (dihedral angle τ ($\angle$(C−Si−Si−C)) = 8.9°; cf. 0.4° for **8** and 0.0° for **1**). The distortion δ is more pronounced in **9** (δ = 171.0°) as compared to that in **1** and **8** (δ = 172.7 and 175.7°, respectively).

Due to its moderate redox strength, **1** should straightforwardly react with suitable organometallic oxidants such as the ferrocenium cation [Fc]$^+$ to give the cationic metallocene **8**. The preparative oxidation of **1** was carried out with 1 equiv of ferrocenium hexafluorophosphate ([Fc][PF$_6$], **10**) in dichloromethane (Scheme 2). The cationic complex **8** was isolated as a yellow-green, air-stable solid in very good yields of 92%. **8** is sparingly soluble in THF but shows a good solubility in more polar solvents such as acetonitrile. Unlike its paramagnetic precursor (**1**), the 18e complex **8** was characterized in solution by multinuclear NMR spectroscopy. The C_5H_4 resonances in the ^{1}H NMR spectrum (CD_3NO_2) at 6.10 (vt) and 5.66 (vt) are significantly shifted to higher frequencies with respect to those reported for the related [2]silaferrocenophane **11** (4.2 ppm, 60 MHz, C_6D_6)[19] and indicate the typical pattern of an AA′BB′ system of monosubstituted aromatic cyclopentadienyl ligands. However, the signal at −4.44 ppm in the ^{29}Si NMR spectrum of **8** for the two equivalent silicon nuclei is comparable to that of the [2]silaferrocenophane **11** (−8.8 ppm).[3g] Solution UV−vis spectra of **8** in methanol were recorded in the range 200−600 nm. Three absorbances were observed at 252 nm (ϵ = 9916 L mol^{-1} cm^{-1}), 289 nm (ϵ = 4541 L mol^{-1} cm^{-1}), and 368 nm (ϵ = 722 L mol^{-1} cm^{-1}). Analogous to the case for the neutral complexes **1** and the carbon-bridged derivatives, a red shift of the lowest energy absorbances λ_{max} of the [2]C-bridged cobaltocenium hexafluorophosphate **12** (422 nm) and the [3]C-bridged cobaltocenium hexafluorophosphate **13** (402 nm) relative to **8** (368 nm) was observed.[4e] However, this red shift was less pronounced for the cationic complexes due to lower molecular strain. More importantly, λ_{max} for the 18e diamagnetic salt **8** is bathochromically shifted by ∼50 nm compared to the 19e paramagnetic analogue **1**. These data suggest an increase of the HOMO−LUMO gap as a result of a decreasing tilt angle (for X-ray studies in the solid state, see below).

In order to obtain potentially relevant data for the behavior of **8** toward strong oxidants and to compare with the results obtained for **1** in THF, we performed additional CV investigations of the cationic complex (**8**) in acetonitrile. The latter was chosen because of the good solubility of **8** and the larger oxidative potential window of CH_3CN as compared to THF. The reduction part of the cyclic voltammogram obtained with **8** in acetonitrile/0.1 M [nBu$_4$N][PF$_6$] as electrolyte is shown in Figure 2 (dotted line). The redox potentials of $E^\circ_{1/2} = -1.34$ V and $E^\circ_{1/2} = -2.29$ V (vs Fc/Fc$^+$) directly correspond to the investigations made for **1**. The latter reduction potential is slightly less negative than observed for **1** in THF and may originate from solvent influences. The first redox wave (i.e., **8** → **1**) centered at $E^\circ_{1/2} = -1.34$ V is slightly less negative compared to [2]C- and [3]C-bridged cobaltocenium salts (**12** and **13**)[4e] and presumably is a result of the different electronic effects excerted by the disilyl bridge (lower LUMO energy).

(19) Kumada, M.; Kondo, T.; Mimura, K.; Ishikawa, M.; Yamamoto, K.; Ikeda, S.; Kondo, M. *J. Organomet. Chem.* **1972**, *43*, 293.

(20) Gennett, T.; Weaver, M. J. *J. Electroanal. Chem. Interfacial Electrochem.* **1985**, *186*, 179.

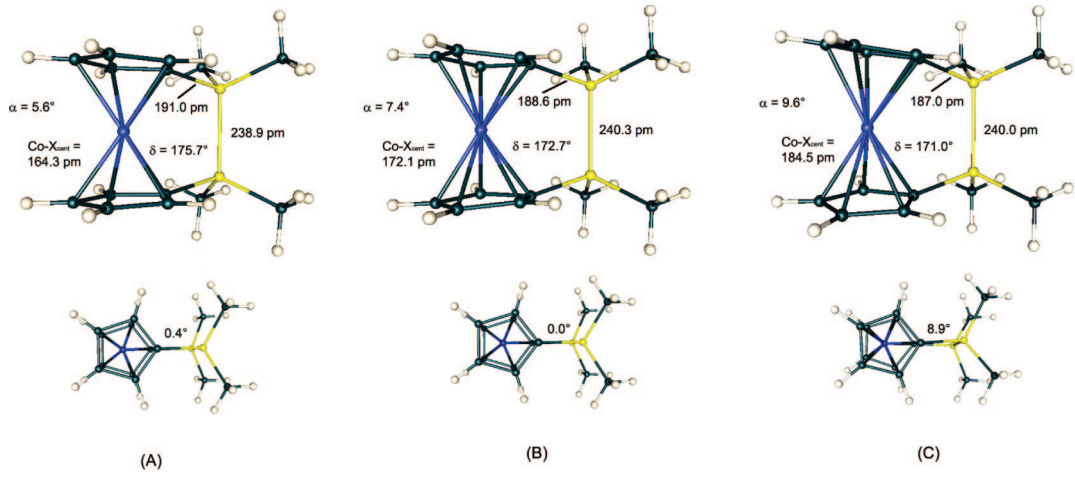

Figure 3. Calculated structures and most important structural parameters of the model compounds **8** (A), **1** (B), and **9** (C) (top) and corresponding top views (bottom). The angles given in the top views represent the dihedral angle τ ($\angle$(C−Si–Si–C)) X_{cent} denotes centroids of the C_5H_4 ligands, the tilt angle α is defined as the angle between the two cyclopentadienyl ring planes, and the distortion δ is defined by the angle $X_{cent}1-M-X_{cent}2$.

Scheme 2. Synthesis of 8

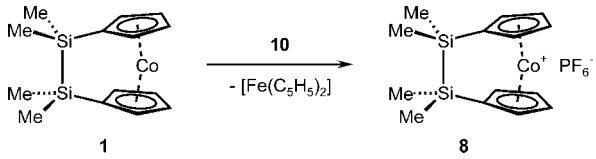

As can be seen from the differences of both peak potentials $\Delta\varphi_p = \varphi_p{}^a - \varphi_p{}^c$ for each redox wave, the kinetics of the individual reduction steps in CH_3CN are slightly different ($\Delta\varphi_p(1) = 74$ mV, $\Delta\varphi_p(2) = 116$ mV).[17] This is in line with previous electrochemical findings suggesting a reduced lifetime of $[Cp_2Co]^-$ in CH_3CN.[16,20] Furthermore, we detected an irreversible redox process at a positive potential of $E^\circ_{1/2} \approx +1.74$ V. The latter can most likely be assigned to an oxidation which is centered at the Si−Si bridge, leading to decomposition and/or polymerization products. This assumption is supported by DFT findings, which predicted the HOMO of **8** to be mainly localized on the bridging Si−Si single bond.

Single crystals of **1** suitable for X-ray diffraction analysis were obtained from a hexane solution at −30 °C. Compound **1** crystallizes in the monoclinic space group $P2_1/m$. The molecular structure of **1** is shown, and selected bond lengths and angles are given in Figure 4.[21]

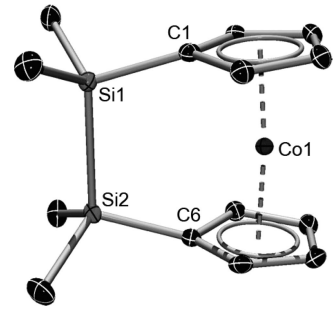

Figure 4. Molecular structure of **1**. Thermal ellipsoids are shown at the 50% probability level. Hydrogen atoms are omitted for clarity. Selected bond lengths (Å) and angles (deg): Si1−Si2 = 2.3737(6), C1−Si1−Si2−C6 = 0.13(7), $X_{cent}1-M-X_{cent}2$ = 173.57 ($X_{cent}1$ and $X_{cent}2$ denote centroids of the C_5H_4 ligands).

Analogous to the case for the parent cobaltocene **4**, the cyclopentadienyl ligands in **1** are η^5-coordinated with Co−C distances ranging from 2.0711(15) to 2.1437(14) Å (**4**: Co−C = 2.079(9)−2.111(8) Å).[22] The aromatic rings display an eclipsed arrangement, indicated by the dihedral angle τ (C1−Si1−Si2−C6) of 0.13(7)°. The values α = 5.98(11)° and δ = 173.57° for **1** indicate the presence of modest molecular strain compared to the case for the undistorted Cp_2Co (**4**: α and δ approximately 0 and 180°, respectively). The recently reported [2]carbacobaltocenophane [$(H_2C)_2(\eta^5$-$C_5H_4)_2Co$] (**2**), however, exhibits a much more pronounced strain (α = 27.1(4)°, δ = 158.0(16)°, τ = 34.53°) due to the significantly shorter E−E bridge (**1**, Si−Si = 2.3737(6) Å, **4**, C−C = 1.554(9) Å).[4e] On the other hand, the corresponding 18e [2]silaferrocenophane (**11**) shows less distortion (α = 4.19(2)°, δ = 176.48(3)°, τ = 8.07(11)°) than **1**, an effect ascribed to the smaller M−C_5H_4 separation in the former (**1**, Co−C = 2.0711(15)−2.1437(14) Å; **11**, Fe−C = 2.027(3)−2.0485(24) Å).[23] Apparently, the d-electron configuration of the metal center is a parameter of significant influence on the overall geometry of closely related *ansa*-metallocenes. In the [2]silaferrocenophane **11** (d^6 iron

(21) The crystal data of **1** and **8** were collected on a Bruker X8Apex diffractometer with a CCD area detector and multi-layer mirror monochromated Mo Kα radiation. The structures were solved using direct methods, refined with the Shelx software package (Sheldrick, G. *Acta Crystallogr. A64*, 112.) and expanded using Fourier techniques. All non-hydrogen atoms were refined anisotropically. Hydrogen atoms were assigned to idealized positions and were included in structure factor calculations. Crystal data for **1**: $C_{14}H_{20}CoSi_2$, M_r = 303.41, brown block, 0.21 × 0.18 × 0.12 mm^3, monoclinic space group $P2_1/m$, a = 8.2595(3) Å, b = 10.3127(5) Å, c = 8.5719(4) Å, β = 90.380(2)°, V = 730.12(6) Å^3, Z = 2, ρ_{calcd} = 1.380 g cm^{-3}, μ = 1.316 mm^{-1}, $F(000)$ = 318, T = 99(2) K, R1 = 0.0180, wR2 = 0.0519, 3843 independent reflections ($2\theta \le 59.12°$) and 159 parameters. Crystal data for **8**: $C_{14}H_{20}CoF_6PSi_2$, M_r = 448.38, yellow needle, 0.23 × 0.12 × 0.05 mm^3, orthorhombic space group *Pbca*, a = 13.1738(5) Å, b = 12.7807(4) Å, c = 21.3933(7) Å, V = 3602.0(2) Å^3, Z = 8, ρ_{calcd} = 1.654 g cm^{-3}, μ = 1.227 mm^{-1}, $F(000)$ = 1824, T = 100(2) K, R1 = 0.0314, wR2 = 0.0774, 3553 independent reflections ($2\theta \le 52.1°$) and 230 parameters. Crystallographic data have been deposited with the Cambridge Crystallographic Data Center as Supplementary Publication Nos. CCDC-685949 and 685950. These data can be obtained free of charge from The Cambridge Crystallographic Data Centre via www.ccdc.cam.ac.uk/data_request/cif.

(22) Buender, W.; Weiss, E. *J. Organomet. Chem.* **1975**, *92*, 65.

(23) (a) Finckh, W.; Tang, B. Z.; Foucher, D. A.; Zamble, D. B.; Ziembinski, R.; Lough, A.; Manners, I. *Organometallics* **1993**, *12*, 823. (b) Dement'ev, V. V.; Cervantes-Lee, F.; Parkanyi, L.; Sharma, H.; Pannell, K. H.; Nguyen, M. T.; Diaz, A. *Organometallics* **1993**, *12*, 1983.

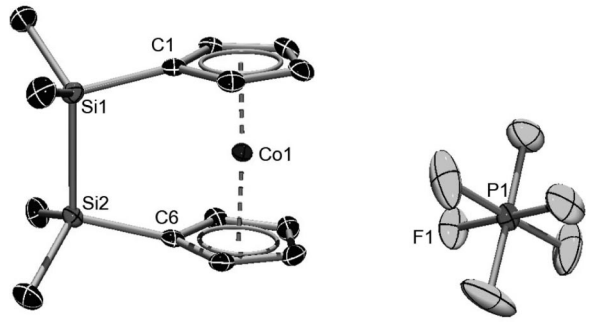

Figure 5. Molecular structure of **8**. Thermal ellipsoids are shown at the 50% probability level. Hydrogen atoms are omitted for clarity. The $[PF_6]^-$ anion was disordered, and only one part is presented in the figure. Selected bond lengths (Å) and angles (deg): Si1−Si2 = 2.3639(7), C1−Si1−Si2−C6 = 9.31(8), $X_{cent}1-M-X_{cent}2$ = 176.65.

center) all occupied molecular orbitals with mainly d character are binding, while in **1** the additional electron of the d^7 cobalt center occupies a molecular orbital with significant antibonding character, thus weakening the M−C_5H_4 bond as reported for the carba-bridged derivative **2**.[4e,23]

For comparison of the solid-state structure of **1** to that of its cationic analogue **8**, single crystals of the latter were grown from a nitromethane solution at room temperature. **8** crystallizes in the orthorhombic space group *Pbca* (Figure 5).[21]

The d^6 Co derivative **8** shows less distortion than **1**, depicted by its structural parameters $\alpha = 3.67(4)°$, $\delta = 176.65°$, and $\tau = 9.31(8)°$, ascribed to the smaller M−C_5H_4 distance (Co−C = 2.0247(18)−2.0374(19) Å) engendered by the d-electron configuration as described before. As is to be expected for isoelectronic metallocenophanes, the structure of complex **8** very much resembles that of its Fe d^6 counterpart **11** (for parameters see above).[23]

To summarize, we have described combined experimental and DFT studies of the first [2]silacobaltocenophane and its oxidation to the corresponding cobaltocenium salt. The electronic characteristics of these complexes were elucidated by using various methods such as EPR spectroscopy and cyclic voltammetry. DFT calculations support the experimental findings. By comparison of the molecular structures and UV−vis spectra the influence of the electronic structure on the overall geometry could be depicted. A significant increase in molecular strain can be engendered by an occupied molecular orbital with significant antibonding character, weakening the M−C_5H_4 bond.

Experimental Section

All reactions and manipulations were carried out under an atmosphere of dry argon with common Schlenk techniques. The solvents were dried with a solvent purification system (SPS) from MBraun and stored under argon over 4 Å molecular sieves; all reagents were dried and purified by standard procedures. $[CoBr_2(dme)]$[24] and 1,2-bis(cyclopentadienyl)-1,1,2,2-tetramethyldisilane[25] were synthesized according to literature procedures. BuLi and ferrocenium hexafluorophosphate were obtained commercially and used without further purification. NMR spectra were recorded on a Bruker Avance 500 NMR spectrometer at 500.13 MHz (^{1}H, external standard TMS), 202.46 MHz (^{31}P, external standard 85% H_3PO_4), 125.77 MHz ($^{13}C\{^1H\}$, external standard TMS) and 99.36 MHz (^{29}Si, external standard TMS). Elemental analyses (C, H, N) were performed on a Leco Instruments Elemental Analyzer, type CHNS 932. UV−vis spectra were recorded on a Shimadzu UV mini 1240 spectrophotometer. Continuous wave (CW) electron paramagnetic resonance spectroscopy was performed at X-band on a Bruker EMXplus spectrometer (microwave frequency 9.43 GHz) equipped with a liquid nitrogen cryostat. The spectra were measured with a modulation amplitude of 10 G and a modulation frequency of 100 kHz, and the field was calibrated by using 2,2-diphenyl-1-picrylhydrazyl (DPPH) with a *g* value of 2.0036. CW EPR simulations were calculated using the Bruker XSophe program package (version 1.1.4). Cyclic voltammetry measurements were performed with an EG&G potentiostat (PAR Model 263A) and an electrochemical cell for sensitive compounds developed by Heinze.[26] We used a freshly polished Pt disk as the working electrode, a Pt wire as the counter electrode, and an Ag wire as the reference electrode ($[nBu_4N][PF_6]$ (0.1 M) as electrolyte). Potentials were calibrated against the Fc/Fc^+ couple, which has a potential of $E°_{1/2}$ = 0.352 V vs Ag/AgCl.

Synthesis of $[(Me_2Si)_2(\eta^5\text{-}C_5H_4)_2Co]$ (1). To a solution of 1.23 g (5.00 mmol) of 1,2-bis(cyclopentadienyl)-1,1,2,2-tetramethyldisilane in 50 mL of toluene/ether (9:1) was added dropwise 6.25 mL (10 mmol, 1.6 M solution in hexanes) BuLi at 0 °C with stirring. The mixture was warmed to room temperature and was stirred for an additional 18 h. The white solid was filtered, washed three times with hexane, and dissolved in 40 mL of THF. The solution was cooled to −78 °C, and 1.54 g (5.00 mmol) of $[CoBr_2(dme)]$ was added. The resulting brown suspension was warmed to ambient temperature and was stirred for 18 h. All volatiles were removed in vacuo, and the residue was extracted with hexane. The solvent of the dark brown solution was evaporated and the crude product sublimed in vacuo. Yield: 0.470 g (1.55 mmol, 31%) of a dark brown solid. Anal. Calcd for $C_{14}H_{20}Si_2Co$: C, 55.42; H, 6.64. Found: C, 55.24; H, 6.67.

Synthesis of $[(Me_2Si)_2(\eta^5\text{-}C_5H_4)_2Co][PF_6]$ (8). A mixture of 150 mg (0.494 mmol) of **1** and 164 mg (0.494 mmol) of ferrocenium hexafluorophosphate **10** was suspended in 5 mL of dichloromethane and the suspension stirred for 30 min. The color of the suspension changed from blue to orange. All volatiles were removed in vacuo, and the residue was washed three times with 5 mL of hexane and dried in vacuo. Yield: 203 mg (0.453 mmol, 92%) of a yellow-green solid. ^{1}H NMR (500.13 MHz, CD_3NO_2): δ 6.10 (vt, 4H, Cp *H*), 5.66 (vt, 4H, Cp *H*), 0.54 (s, 12H, $SiMe_2$). ^{13}C NMR (CD_3NO_2): δ 100.33 (C_{ipso} Cp), 89.38 (*C* Cp), 87.30 (*C* Cp), −3.28 ($SiMe_2$). ^{29}Si NMR: δ −4.44 ($SiMe_2$). ^{31}P NMR: δ −144.70 (sept, J_{P-F} = 1746.9 Hz, PF_6). Anal. Calcd for $C_{14}H_{20}Si_2PF_6Co$: C, 37.50; H, 4.50. Found: C, 37.31; H, 4.69.

Theoretical Formalism and Computational Details. Structure Optimization and Generation of Wave Functions for EPR Parameter Ccalculations. The optimizations for **1**−**3** and for Cp_2Co (**4**) were carried out with Turbomole 5.9[27] using RIDFT at the BP86[28]/def2-TZVP[29] level. Analytical frequency calculations[30] were performed at the same level and represent true minima without imaginary frequencies on the respective potential-energy surface. The anionic complex **3** was initially optimized in a singlet ground state but showed one imaginary frequency at −50

(24) Fowles, G. W. A.; Rice, D. A.; Walton, R. A. *J. Inorg. Nucl. Chem.* **1969**, *31*, 3119.
(25) Jutzi, P.; Krallmann, R.; Wolf, G.; Neumann, B.; Stammler, H. G. *Chem. Ber.* **1991**, *124*, 2391.
(26) (a) Hinkelmann, K.; Heinze, J.; Schacht, H.-T.; Field, J. S.; Vahrenkamp, H. *J. Am. Chem. Soc.* **1989**, *111*, 5078. (b) Heinze, J. *Angew. Chem.* **1984**, *96*, 823 *Angew. Chem., Int. Ed.* **1984**, *23*, 831.
(27) (a) Ahlrichs, R.; Bär, M.; Häser, M.; Horn, H.; Kölmel, C. *Chem. Phys. Lett.* **1989**, *162*, 165. (b) Treutler, O.; Ahlrichs, R. *J. Chem. Phys.* **1995**, *102*, 346. (c) Sierka, M.; Hogekamp, A.; Ahlrichs, R. *J. Chem. Phys.* **2003**, *118*, 9136. (d) Ahlrichs, R. *Phys. Chem. Chem. Phys.* **2004**, *6*, 5119.
(28) (a) Becke, A. D. *Phys. Rev. A* **1988**, *38*, 3098. (b) Perdew, J. P. *Phys. Rev. B* **1986**, *33*, 8822.
(29) (a) Weigend, F.; Ahlrichs, R. *Phys. Chem. Chem. Phys.* **2005**, *7*, 3297. (b) Weigend, F. *Phys. Chem. Chem. Phys.* **2006**, *8*, 1057.
(30) Deglmann, P.; Furche, F.; Ahlrichs, R. *Chem. Phys. Lett.* **2002**, *362*, 511.

cm^{-1}. Subsequent geometry optimizations of the corresponding triplet ground state revealed a true minimum (no imaginary frequency) that was ~62.9 kJ mol^{-1} (incl. ZPE) lower in energy than the singlet state. Since the theoretical treatment of anionic species (such as **3**) is often problematic, we have performed consistently additional optimization steps on **1**−**3** using an appropriate "solvent cage" approximation (conductor-like screening model (Cosmo) in CH_3CN ($\varepsilon = 36.64$)).[31] Details such as the complete list of coordinates, frequency analyses, and energies of the calculated species are compiled in the Supporting Information.

Unrestricted Kohn−Sham single-point calculations for EPR parameter calculations were subsequently performed with Turbomole 5.9[27] using a 9s7p4d basis set for cobalt (specifically designed for hyperfine calculations)[13,32] and flexible IGLO-II[33] basis sets for the ligand atoms. The following DFT exchange-correlation functionals were compared: (a) the GGA functional BLYP[34] and the hybrid functionals (b) B3LYP[34,35] with 20% exact exchange and (c) BHLYP[34,36] with 50% exact exchange, as well as the user-defined hybrid functionals (d) B-30LYP with 30% exact exchange (70% E_x^{Slater} and 70% ΔE_x^{B88} and E_c^{LYP}) and (e) B-40LYP with 40% exact exchange (60% E_x^{Slater} and 60% ΔE_x^{B88} and E_c^{LYP}).

The unrestricted Kohn−Sham orbitals were transferred to the MAG-Respect property package[37] by suitable interface routines. The atomic mean-field approximation (AMFI)[38] has been used to compute the matrix elements of the spin−orbit (SO) operator h_{SO} in eq 3.

Hyperfine Tensor Calculations. In the usual nonrelativistic first-order approximation, isotropic hyperfine splittings $a_{iso}(N)$ correspond to the Fermi-contact term A_{FC}:

$$a_{iso}(N) = \mathbf{A}_{FC} = \frac{4\pi}{3}\beta_e\beta_N g_e g_N \langle S_z\rangle^{-1} \sum_{\mu,\nu} P_{\mu,\nu}{}^{\alpha-\beta} \langle \varphi_\mu|\delta(\mathbf{R}_N)|\varphi_\nu\rangle \quad (1)$$

Here β_e is the Bohr magneton, β_N the nuclear magneton, g_N is the g value of nucleus N, $\langle S_z\rangle$ is the expectation value of the z component of the total electronic spin, $P_{\mu,\nu}{}^{\alpha-\beta}$ is the spin density matrix, and the summation runs over all occupied molecular orbitals. The components $T_{ii}(N)$ of the anisotropic tensor are given by

$$T_{ii}(N) = \frac{1}{2}\beta_e\beta_N g_e g_N \langle S_z\rangle^{-1} \sum_{\mu,\nu} P_{\mu,\nu}{}^{\alpha-\beta} \langle \varphi_\mu|\mathbf{r}_N{}^{-5}(\mathbf{r}_N{}^2\delta_{ij} - 3\mathbf{r}_{N,i}\mathbf{r}_{N,j})|\varphi_\nu\rangle \quad (2)$$

where $\mathbf{r}_N = \mathbf{r} - \mathbf{R}_N$ ($\mathbf{R}_N$ is the position vector of nucleus N). In the rest of this section, we will refer to the metal hyperfine interaction and omit subscript N. The second-order perturbation treatment of ref 39 is used to compute spin−orbit (SO) corrections to the hyperfine tensor. At the coupled-perturbed Kohn−Sham level, the dominant SO correction term arises as a second-order cross term between the one- and two-electron SO Hamiltonian H^{SO} and the perturbed Fock operator F'

$$\mathbf{A}_{K,u\nu}{}^{SO-I} = \frac{1}{2}\alpha^4 g_e \gamma_K \frac{1}{2\langle S_z\rangle} \times \sum_k^{occ(\alpha)} \sum_a^{virt(\alpha)} \frac{\langle \Psi_k{}^\alpha|h_u{}^{SO}|\Psi_a{}^\alpha\rangle \langle \Psi_a{}^\alpha|F'_\nu|\Psi_k{}^\alpha\rangle}{\varepsilon_k{}^\alpha - \varepsilon_a{}^\alpha} - \sum_k^{occ(\beta)} \sum_a^{virt(\beta)} \frac{\langle \Psi_k{}^\beta|h_u{}^{SO}|\Psi_a{}^\beta\rangle \langle \Psi_a{}^\beta|F'_\nu|\Psi_k{}^\beta\rangle}{\varepsilon_k{}^\beta - \varepsilon_a{}^\beta} \quad (3)$$

where α is the fine-structure constant, γ_K the gyromagnetic ratio of the nucleus, h^{SO} is the one- and two-electron spin−orbit operator, F' is the perturbed Fock operator, with $F'_\nu = (l_\nu/r^3) - (2)/(\alpha)a_0 \sum_{k=1}^{n/2} K'_\nu$, where l_ν/r^3 is the paramagnetic nuclear-spin electron-orbit (PSO) operator, K'_ν is a component of the response exchange operator, and a_0 is the weight of HF exchange depending on the specific hybrid functional used (see ref 40 for a related simultaneous CPKS implementation and also ref 39 for references to earlier work). ψ^σ and ε^σ are spin-polarized Kohn−Sham orbitals and orbital energies, respectively. GGA and LDA functionals lead to an uncoupled DFT (UDFT) treatment for this second-order term ($a_0 = 0$).

g-Tensor Calculations. The **g** tensor will be provided as correction to the free-electron value g_e (in ppt, i.e. in units of 10^{-3})

$$g = g_e + \Delta g \quad (4)$$

with $g_e = 2.002\,319$. Up to the level of second-order perturbation theory based on the Breit−Pauli Hamiltonian, the g shift Δg consists of three terms:

$$\Delta g = \Delta g^{SO/OZ} + \Delta g^{RMC} + \Delta g^{GC} \quad (5)$$

of which the "paramagnetic" second-order spin−orbit/orbital Zeeman cross term, $\Delta g^{SO/OZ}$, dominates (except for extremely small Δg values).[40] The relativistic mass correction term Δg^{RMC} and the one-electron part of the gauge correction term Δg^{GC} are also included in our implementation.[41]

Acknowledgment. We are grateful for financial support from the DFG and the Fonds der Chemischen Industrie. We thank Dr. Jeffrey Harmer for valuable discussions.

Supporting Information Available: CIF files giving X-ray structural data and tables giving detailed lists of coordinates, frequency analyses, and energies of the calculated species. This material is available free of charge via the Internet at http://pubs.acs.org.

OM8003724

(31) (a) Klamt, A.; Schüürmann, G. *J. Chem. Soc., Perkin Trans. 2* **1993**, *5*, 69. (b) Lide, D. R., Ed. *CRC Handbook of Chemistry and Physics*, 77th ed.; CRC Press: Boca Raton, FL, 1997.

(32) (a) Munzarová, M.; Kubácek, P.; Kaupp, M. *J. Am. Chem. Soc.* **2000**, *122*, 11900. (b) Schäfer, A.; Horn, H.; Ahlrichs, R. *J. Chem. Phys.* **1992**, *97*, 2571.

(33) (a) Huzinaga, S. Ph.D. Thesis, University of Alberta, Edmonton, Alberta, Canada, 1971. (b) Kutzelnigg, W.; Fleischer, U.; Schindler, M. In *NMR Basis Principles and Progress*; Diehl, P., Ed.; Springer-Verlag: Heidelberg, Germany, 1990; Vol. 23.

(34) Becke, A. D. *J. Chem. Phys.* **1993**, *98*, 5648.

(35) Stephens, P. J.; Devlin, F. J.; Chabalowski, C. F.; Frisch, M. J. *J. Phys. Chem.* **1994**, *98*, 11623.

(36) Lee, C.; Yang, W.; Parr, R. G. *Phys. Rev. B* **1988**, *37*, 785.

(37) Malkin, V. G.; Malkina, O. L.; Reviakine, R.; Arbouznikov, A. V.; Kaupp, M.; Schimmelpfennig, B.; Malkin, I.; Helgaker, T.; Ruud, K. MAG-Respect, Version 1.2, 2003.

(38) (a) Hess, B. A.; Marian, C. M.; Wahlgren, U.; Gropen, O. *Chem. Phys. Lett.* **1996**, *251*, 365. (b) Schimmelpfennig, B. Ph.D. Thesis, Stockholms Universitet, 1996.

(39) (a) Arbouznikov, A. V.; Vaara, J.; Kaupp, M. *J. Chem. Phys.* **2004**, *120*, 2127. (b) Remenyi, C.; Reviakine, R.; Arbuznikov, A. V.; Vaara, J.; Kaupp, M. *J. Phys. Chem. A* **2004**, *108*, 5026.

(40) Harriman, J. E. *Theoretical Foundations of Electron Spin Resonance*; Academic Press: New York, 1978.

(41) (a) Kaupp, M.; Reviakine, R.; Malkina, O. L.; Arbouznikov, A. V.; Schimmelpfennig, B.; Malkin, V. G. *J. Comput. Chem.* **2002**, *23*, 794. (b) Malkina, L.; Vaara, J.; Schimmelpfennig, B.; Munzarová, M.; Malkin, V. G.; Kaupp, M. *J. Am. Chem. Soc.* **2000**, *122*, 9206.